Design and on-orbit operation of the soft x-ray spectrometer adiabatic demagnetization refrigerator on the Hitomi observatory

Peter John Shirron
Mark O. Kimball
Bryan L. James
Theodore Muench
Edgar R. Canavan
Michael J. DiPirro
Thomas A. Bialas
Gary A. Sneiderman
Kevin R. Boyce
Caroline Anne Kilbourne
Frederick S. Porter
Ryuichi Fujimoto
Yoh Takei
Seiji Yoshida
Kazuhisa Mitsuda

SPIE.

Design and on-orbit operation of the soft x-ray spectrometer adiabatic demagnetization refrigerator on the Hitomi observatory

Peter John Shirron,[a,*] Mark O. Kimball,[a] Bryan L. James,[a] Theodore Muench,[a] Edgar R. Canavan,[a] Michael J. DiPirro,[a] Thomas A. Bialas,[a] Gary A. Sneiderman,[a] Kevin R. Boyce,[a] Caroline Anne Kilbourne,[a] Frederick S. Porter,[a] Ryuichi Fujimoto,[b] Yoh Takei,[c] Seiji Yoshida,[d] and Kazuhisa Mitsuda[c]

[a]NASA/Goddard Space Flight Center, Greenbelt, Maryland, United States
[b]Kanazawa University, Kanazawa, Ishikawa, Japan
[c]ISAS/JAXA, Sagamihara, Kanagawa, Japan
[d]Sumitomo Heavy Industries, Ltd., Niihama, Ehime, Japan

Abstract. The soft x-ray spectrometer (SXS) instrument that flew on the Astro-H observatory was designed to perform imaging and spectroscopy of x-rays in the energy range of 0.2 to 13 keV with a resolution requirement of 7 eV or better. This was accomplished using a 6×6 array of x-ray microcalorimeters cooled to an operating temperature of 50 mK by an adiabatic demagnetization refrigerator (ADR). The ADR consisted of three stages to operate using either a 1.2 K superfluid helium bath or a 4.5 K Joule–Thomson (JT) cryocooler as its heat sink. The design was based on the following operating strategy. After launch, while liquid helium was present (cryogen mode), two of the ADR's stages would be used to single-shot cool the detectors, using the helium as a heat sink. When the helium was eventually depleted (cryogen-free mode), all three ADR stages would be used to continuously cool the helium tank to about 1.5 K and to single-shot cool the detectors (to 50 mK), using the JT cryocooler as a heat sink. The Astro-H observatory, renamed Hitomi after its successful launch in February 2016, carried ~36 L of helium into orbit. Based on measurements during ground testing, the average heat load on the helium was projected to be 0.66 mW, giving a lifetime of more than 4 years. On day 5, the helium had cooled to <1.4 K and ADR operation began, successfully cooling the detector array to 50 mK. The ADR's hold time steadily increased to 48 h as the helium cooled to a temperature of 1.12 K. As the commissioning phase progressed, the ADR was recycled (requiring ~45 min) periodically, either in preparation for science observations or whenever the 50 mK stage approached the end of its hold time. In total, 18 cycles were completed by the time an attitude control anomaly led to an unrecoverable failure of the satellite on day 38. This paper presents the design, operation, and on-orbit performance of the ADR in cryogen mode as the foreshortened mission did not provide an opportunity to test cryogen-free mode. © *The Authors. Published by SPIE under a Creative Commons Attribution 3.0 Unported License. Distribution or reproduction of this work in whole or in part requires full attribution of the original publication, including its DOI.* [DOI: 10.1117/1.JATIS.4.2.021403]

1 Introduction

The SXS instrument[1] on the Hitomi observatory[2] was a high-resolution imaging spectrometer designed to measure the energy of individual photons in the soft x-ray band (0.2 to 13 keV). Imaging was accomplished using a 6×6 array of microcalorimeters[3] located at the focal point of a grazing-incidence x-ray telescope.[4] Each pixel in the array was able to resolve photon energies to a resolution of better than 5 eV. This resolution was achieved in part by operating the array at a very low temperature, 50 mK, using a three-stage adiabatic demagnetization refrigerator (ADR) whose operation was supported by a cryogenic system[5] consisting of a 40-L superfluid helium tank (at <1.3 K) and a 4.5 K Joule–Thomson (JT) cryocooler, with additional two-stage Stirling cryocoolers[6,7] used to cool vapor-cooled-shields and provide precooling for the JT stage.

The ADR was configured so that it could use either the superfluid helium or the JT cryocooler as its heat sink. The strategy was to launch with 30+ L of liquid helium and initially operate the ADR in "cryogen mode," where it rejected heat directly to the helium. Operation would have continued until the liquid helium was exhausted, then transitioned to a "cryogen-free mode" where the ADR assumed the additional task of cooling the (empty) helium tank while rejecting heat to the JT cryocooler. The ADR's design and performance in these two operating modes have been reported previously.[8–11] This paper summarizes the ADR's design and operating parameters and reports on its performance during the 38 days that the instrument was operational in orbit before an anomaly ended the mission.[12] A companion paper describes the operation and performance in cryogen-free mode observed during ground testing.[10]

*Address all correspondence to: Peter John Shirron, E-mail: peter.shirron@nasa.gov

2 Adiabatic Demagnetization Refrigerator Design, Operation and Ground Test Performance

2.1 Adiabatic Demagnetization Refrigerator Requirements and Design Summary

Top-level and selected derived requirements for the SXS ADR are shown in Table 1. The requirements that relate directly to detector performance, such as operating temperature, temperature stabilities, and instrument observing efficiency, are the same in both operating modes. Requirements that relate to heat flows between the detectors, ADR, and heat sinks differ for the two modes as they reflect differences in operating temperatures of the helium tank (which dictates the detector heat load to the ADR) and differences in how the heat sinks (stored cryogen versus cryocooler) operate. Concerning the latter, the helium tank has a lifetime determined by the time average heat load, and the JT cryocooler has a maximum cooling power of 40 mW at 4.5 K. Consequently, in cryogen mode, it is most important to constrain the ADR's time average heat rejection to the liquid helium, whereas in cryogen-free mode it is most important to constrain its peak reject rate to the JT cooler.

Table 1 also lists the design parameters for the ADR's three stages that are most relevant to thermodynamic performance.

CPA is chrome potassium alum and GLF is gadolinium lithium fluoride.

2.2 Mechanical and Thermal Configuration

The ADR's stages are arranged to make both mechanical and thermal connections to the helium tank and the JT cryocooler, as shown in Fig. 1 (which is a subset of the SXS cryogenic system). The particular distribution was based on the need to achieve fault tolerance. That is, the SXS instrument must be able to achieve its science goals with a premature failure of the liquid helium or of the JT cryocooler. (Since the SXS instrument was not required to be two-fault tolerant, failures of other cryocoolers are considered only in the context of fully operational helium and JT systems.) A failure of the liquid helium with a functional JT cryocooler simply requires a transition to cryogen-free mode. A failure of the JT cryocooler, however, would result in its temperature rising above 10 K, and any ADR stage thermally attached to it would not be operable. Since ADR stages 1 and 2 must be operable in cryogen mode, both stages (i.e., their magnets) must be thermally attached to the helium tank, even though there would be significant performance advantages in cryogen-free mode to having stage 2 attached to the JT cryocooler.

Table 1 Requirements, and design and operating parameters for the three-stage SXS ADR.

Performance requirements		
	Cryogen mode	Cryogen-free mode
Detector operating temperature (K)	0.05	0.05
Detector temperature stability (μK rms)	2.5	2.5
Detector housing temperature stability (mK)	1.0	1.0
Detector heat load (μW)	0.27	0.47
Minimum observing efficiency	90%	90%
-Typical hold time (hours)	24	15
-Typical recycle time (hours)	1	2
Maximum heat sink load (mW)	0.2 (avg)	30 (peak)
Maximum magnetic field at detectors (mT)	10	10

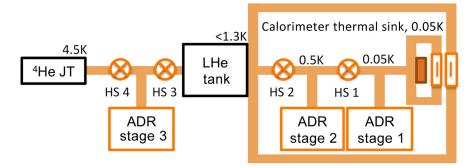| Physical design parameters			
	Stage 1	Stage 2	Stage 3
Refrigerant type	CPA	GLF	GLF
Refrigerant mass (g)	270	147	147
Maximum magnetic field (T)	2	3	3
Maximum magnet current (A)	2	2	2
Maximum magnet voltage (V)	±1	±1	±1
Magnet inductance (H)	250	200	200

Fig. 1 Thermal schematic of the subset of the Hitomi cryogenic consisting of the ADR, helium tank, and JT cryocooler.
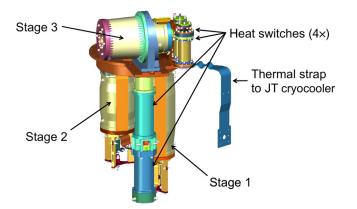

Fig. 2 Solid model representation of the SXS three-stage ADR.

Figure 2 shows a solid model representation of the ADR assembly. The four heat switches (HS 1 to HS 4) are active gas-gap. The ADR and detector assembly are an integral unit that was inserted into a well in the top end of the helium tank, with the central mounting plate serving as both a mechanical and thermal interface to the helium tank.

2.3 Adiabatic Demagnetization Refrigerator Control Electronics

The ADR control electronics (ADRC) use 2-quadrant voltage-source power supplies for regulating the current in each stage's magnet and can exert either open-loop or closed-loop control. In open-loop control, programmable voltages are applied to the magnet, whereas in closed-loop control, the magnet voltage is the calculated output of a proportional-integral-derivative (PID) feedback loop. In both cases, magnet voltage is limited to values in the range of -1 to $+1$ V, and the current to values between 0 and $+2.00$ A. The ADR stages are nearly always in closed-loop control. Open-loop control is used only for stage 1 as it demagnetizes to its hold temperature, giving time for the PID circuit to switch control thermometers from a Cernox™ 1030[13] having good resolution at temperatures above about 0.3 K to a germanium resistance thermometer (GR-200A-30[13]) preselected by the vendor for high dR/dT at 50 mK.

2.4 Adiabatic Demagnetization Refrigerator Recycling

As mentioned previously, in cryogen mode, only stages 1 and 2 are needed to cool the detector array to 50 mK. The recycling

process can be triggered either by ground command or automatically when stage 1's current falls below a preset threshold during its 50-mK hold. The recycling sequence was optimized to yield the shortest recycle time rather than, for example, best thermodynamic efficiency.

To recycle the ADR, the first step is to magnetize the two stages by setting their control setpoints to a temperature above that of the helium tank. When stage 2 warms above the tank, heat switch HS2 is powered on, and as stage 1 warms above stage 2, heat switch HS1 is powered on. Closed-loop control eventually results in both magnets reaching their peak current of 2 amps, and both stages cooling as they equilibrate with the helium tank. When stage 2 cools below a preset threshold (1.4 K), heat switch HS2 is powered off, and stage 2's control setpoint is gradually lowered so that it steadily cools stage 1. When stage 1 cools below its preset threshold of 0.75 K, heat switch HS1 is powered off.

Stages 1 and 2 are then demagnetized by commanding their control setpoints to the desired hold temperatures, 50 mK and 0.5 K, respectively. After stable control is obtained, the stages are steadily demagnetized to maintain temperature as they absorb heat.

Figure 3 shows (a) the temperatures and (b) currents of stages 1 and 2 during a typical recycle during ground tests. The time required for each recycle, and the amount of heat that must be rejected, depend on the starting currents and temperatures. Except for the initial cycle after launch where the salt pills start at the bath temperature and zero current, a recycle typically begins with the ADR stages at their hold temperatures (50 mK and 0.5 K), and the magnets have only some small residual current. For these starting conditions, the time was just over 45 min.

After a recycle, the instrument requires an equilibration period during which temperatures and heat flows stabilize within the ADR, the detector array and its housing and the detectors reach their ultimate resolution. Equilibration to 50 mK was rapid within the ADR stage, but within the detector array the equilibration times were much longer due to the anomalously large heat capacity of stainless steel fasteners (at temperatures below 100 mK) and the relatively low thermal conductivity of the detector array's cold frame. Another source of long-term drift within the detectors arose from ohmic heating in the resistive portion of the ADR's magnet leads. That heating raised the temperature of the dewar's inner vapor-cooled shield, which thermally coupled to the detector array through the JFET amplifier assembly. Although the coupling is weak, it would lead to time-varying heat flows between the detector array and stage 1 salt, and internal thermal gradients between the
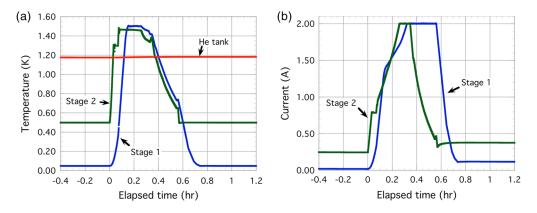
Fig. 3 (a) Temperatures and (b) magnet currents during an ADR recycle (ground test data).

detector array and its control thermometer, whose effect could not be removed by the temperature control system. In practice, the time required for all temperatures to reach the stability level needed for detector operation was 20 to 25 min.

2.5 Adiabatic Demagnetization Refrigerator Cooling Capacities and Performance During Ground Testing

The subsequent hold time at 50 mK depended on the cooling capacity of stage 1's salt pill and the total heat load it had to absorb. The cooling capacity can be calculated from known entropy functions for CPA,[14] the temperature and magnetic field from which it is demagnetized, and the temperature of the salt during the hold (which is necessarily lower than the 50 mK detector control point). A detailed thermodynamic analysis of the SXS ADR has been published previously.[9,15] In this discussion, only a top-level summary is provided.

When stage 1 is demagnetized, as described in the previous section, from 0.75 K and a magnetic field of 2 T (averaged over the volume of the salt pill), the theoretical cooling capacity at 50 mK is 0.165 J. The "realizable" cooling capacity is reduced by inevitable inefficiencies: (1) cooling capacity used during demagnetization to cool nonzero heat capacities, (2) thermal gradients within the salt pill (primarily between the salt and the thermal bus on which it is grown), and (3) thermal gradients between the 50 mK control point and the salt pill's thermal bus.

The realizable cooling capacity is the product of the salt pill's heat load and the hold time at that load (time from first reaching 50 mK until the current reduces to zero). The heat load can be experimentally determined by applying a comparable amount of heat using a heater and noting the difference in demagnetization rate at the same magnet current. By this method, the cooling capacity of stage 1 at 50 mK was determined to be 0.132 J, or 84% of the theoretical capacity.[15] Once the heat absorption efficiency was determined, both salt temperature and heat load could be inferred for any subsequent ADR cycle by fitting the magnet current as a function of time during the 50 mK hold to calculated values that would produce a constant increase in entropy.[14] This analysis consistently yielded a salt temperature of 48.5 mK.

To assess the ADR's performance against requirements, we first note that stage 1's heat load and hold time depended on helium tank temperature, with a dependence of approximately $1/T_{\text{tank}}^{2.138}$. During ground tests, the typical tank temperature was 1.24 K, for which the heat load to stage 1 was 0.88 μW, giving a

hold time of ~41.7 h (74% margin on the design value of 24 h). The critical requirement, though, is the instrument's observing efficiency which is defined as $(\Delta t_{\text{hold}} - \Delta t_{\text{stabilization}})/(\Delta t_{\text{hold}} + \Delta t_{\text{recycle}})$. With $\Delta t_{\text{hold}} = 41.7$ h, $\Delta t_{\text{stabilization}} = 0.5$ h, and $\Delta t_{\text{recycle}} = 0.75$ h, the instrument demonstrated an observing efficiency of about 96.0%, significantly above the 90% requirement.

To determine the average heat rejection rate to the liquid helium, we relied on calorimetric measurements[15] of each contribution to the heat rejected: heat from salt pills, heat used to power the heat switches, and hysteresis heat from the magnets and magnetic shields. The total heat rejected per total ADR cycle (recycle operation and hold time) was ~11.7 J. This heat is rejected every ~42.5 h for a time average rate of 0.071 mW, well below the requirement of 0.20 mW (based on a 3-year lifetime requirement and a minimum volume of 30 L of superfluid helium).

2.6 Detector Temperature Stability

As shown in Table 1, two temperature stability requirements are levied on the SXS instrument. First, the detector array required a stability of 2.5 μK rms or better at 50 mK. Second, the housing that supported the detector array had to be kept stable to within 1-mK rms on timescales of 0.2 sec to 10 min. The second requirement arose from that fact that changes in heat flow along the lead wires and Kevlar suspensions that link the array to the helium tank could cause changes in detector gain. Since the detector array temperature was actively controlled by the ADR and its control electronics, the first stability requirement was levied against those subsystems. In cryogen mode, with the detector housing thermally coupled to the liquid helium, its temperature was passively stabilized over the relevant timescales to by the large heat capacity of the liquid to better than 0.2 mK rms.

Figure 4 shows the typical 50-mK stability level achieved during ground testing. In spite of infrequent disturbances presumably due to cosmic ray events, both short- and long-term stabilities are better than 0.5 μK rms, well below the requirement.

3 On-Orbit Operation and Performance

3.1 Adiabatic Demagnetization Refrigerator Hold Time and Duty Cycle

The final helium tank top off prior to the launch of Hitomi resulted in a fill level of ~38.0 L at 1.2 K. Prelaunch operations
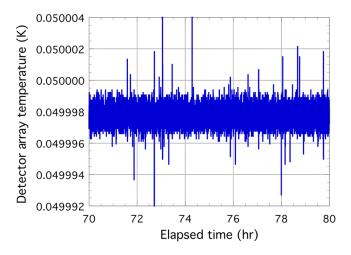
Fig. 4 Typical detector array temperature during ground testing at 50 mK.

required periods during which the cryocoolers were powered down and the helium was not being evacuated. The first telemetry after launch showed the temperature at 1.5 K, which peaked shortly after the cryocooler was powered on. The ADR's control electronics used internal thresholds that required the liquid helium to be <1.4 K before the ADR could cycled. That temperature was reached on day 5, at which point the first ADR cycle was started.

For the first cycle, with the relatively warm helium tank (1.4 K), the heat load to stage 1's salt pill was ~1.06 μW. Based on the ground test characterization, this heat load should yield a hold time of 35 h. The first cycle was terminated 32.5 h by a commanded recycle. As the helium continued to cool and recycles were commanded based either on planned observations or when the end of a hold time was approaching, the heat load to stage 1 continued to decrease and the hold times lengthened.

In total, 18 ADR cycles were completed before the Hitomi satellite went into safe-hold and ceased operation. The demagnetization curves for stage 1 for those 18 ADR cycles are shown
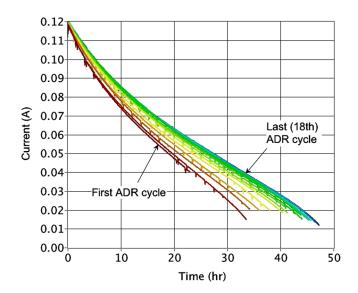

Fig. 5 Demagnetization curves for stage 1 for the 18 cycles completed on orbit. Time is from the first crossing of 50 mK after recycling. The exponential approach of the helium tank to its steady-state temperature gave rise to a gradual increase in hold time with each cycle.

in Fig. 5. The steady cooling of the helium and its effect on ADR performance can be seen as a progressive elongation of the hold time from the first cycle, when the helium was 1.4 K, until the last, when the helium had stabilized at 1.125 K. For the latter cycles, the hold time was ~48 h, yielding an ADR duty cycle of >98. As defined previously, this would imply an observing efficiency of nearly 97.5%, but, as discussed in the next section, periods of instability in the detector array temperature significantly reduced the useful observing time.

3.2 Detector Temperature Stability

One notable feature of the demagnetization curves is periodic dips in current that correlated with the Hitomi observatory passing through the south Atlantic anomaly (SAA). Each day, roughly half of the satellite's ~15 orbits passed through some portion of the SAA, subjecting the SXS to an excess of high-energy particles for up to 15 min. The effect is seen more clearly in the detector array temperature (Fig. 6), which exhibits infrequent, random pulses outside the SAA but an almost continuous stream of pulses within the SAA. The primary effect appears to be high-energy particle strikes within the thermometers-sensing element, based on the fact that the temperature rise was far larger than one would expect from the energy deposited as particles traversed the salt pill or any other cold mass, and the fact that the temperature recovers within seconds. The negative temperature excursions result from the ADR's control electronics responding to the temperature pulses and demagnetizing the stage to keep the (apparent) temperature at an average of 50 mK. This reaction creates the dips in magnet current as shown in Fig. 5.

Although the temperature and magnet current appear to recover after the observatory exits the SAA, there was a cumulative energy deposition that results in a slight offset in current (and entropy) and an increase in the salt pill's time-average heat load. On long (many orbit) timescales, the increase calculated from the corresponding entropy change and the average daily rate of SAA passes was 20 to 30 nW.

During time periods where Hitomi's orbit included even the fringes of the SAA, the detector temperature significantly exceeded the stability requirement, rendering the data unusable for science purposes. When Hitomi's orbit did not overlap with any portion of the SAA, the temperature stability was about 2.0 μK rms—notably higher than seen during ground testing but within the requirement. Using the temperatures shown in Fig. 6, the fraction of time in which the detectors were nominally at 50 mK and where the stability met the 2.5 μK rms requirement was about 76%. This is perhaps a truer measure of the instrument's observing efficiency, although it obscures the fact that the SXS hardware itself demonstrated an ability to achieve observing efficiencies above 97%.

3.3 Stage 1 Heat Load at 50 mK

Although the ADR's hold time and duty cycle were consistent (as required) with an observing efficiency of ≥90%, it is important to assess whether its thermodynamic performance on orbit differed in any way from ground observations. The parameter of greatest interest in this assessment is the heat load to stage 1 at 50 mK. During ground testing, it was possible to determine the heat load by applying an additional heat load using a heater attached to the salt pill. Unfortunately, the flight electronics did not have the capability to control the heater. Instead, we
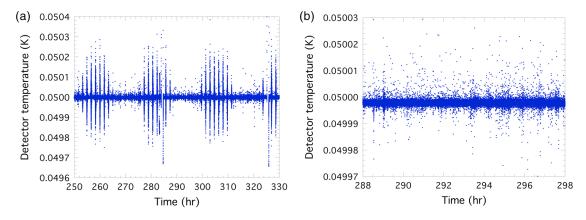
Fig. 6 Detector array temperature (a) showing the effect of high-energy particles during passes through the SAA, and (b) when Hitomi was outside the region of the SAA.

used the fitting method described in Sec. 2.5 for extracting heat loads and salt temperatures from the demagnetization curves shown in Fig. 5. We note, however, that this method implicitly assumes that salt pill's cooling capacity and heat absorption efficiency are unchanged from ground testing. Any change in, for example, the thermal contact of the salt to its thermal bus due to launch loads would yield an apparent increase in heat load. We also note that the fitting excluded the portions of the curves strongly affected by the SAA. The resulting heat loads, therefore, excluded the SAA contribution so that a direct comparison with ground test values could be made.

The results of this analysis, presented in Fig. 7, show an excess heat load to stage 1 during the first 9 or so ADR cycles, whereas for subsequent cycles the heat load was consistent with values observed during ground testing. Without implying a causal connection, we note that during the first nine cycles, the helium tank was approaching the equilibrium temperature of 1.12 K (see Fig. 8) from which all subsequent cycles were conducted.

In Fig. 7, the inferred heat loads are shown (left-hand plot) as a function of the average helium tank temperature during the hold time and (right-hand plot) as a function of the elapsed time (from launch) at which the hold time started. In both cases, the expected heat load based on ground testing is shown as a solid line. Both plots show the expected trend toward lower heat loads as the helium cooled over time. The left-hand

plot shows an offset in heat load that appears relatively constant until the tank cools below 1.15 K, at which point it diminishes to zero. The right-hand plot is more suggestive of an initial excess heat load, which diminishes gradually over time.

Returning to the concern that the salt pill's thermodynamic performance may have changed between ground testing and the start of orbit operations, the eventual agreement between ground test and orbit heat loads suggests that this was a transient effect and not due to (permanent) degradation of the salt pill. As possible transient effects, we have considered (1) vibrational heating in the instrument during launch, (2) cooling of the dewar main shell from 290 K at launch to an eventual equilibrium temperature of ∼260 K, and (3) microphonic heating due to vibration of the dewar main shell (for example, from the cryocooler compressors).

As a root cause, vibrational heating during launch (#1) is highly unlikely given that the instrument was subjected to harsher vibration testing at the spacecraft level, and postvibration testing showed no short- or long-term effect on heat loads. Cooling of the main shell on orbit (#2) could lead to short- and long-term drifts in internal temperatures and heat flows as the system stabilizes. While this cooling should result in a "reduction" in heat loads from those observed in ground tests, such reductions combined with elevated heat loads during passes through the SAA could generate the appearance of having an elevated heat load that disappears over time. But this

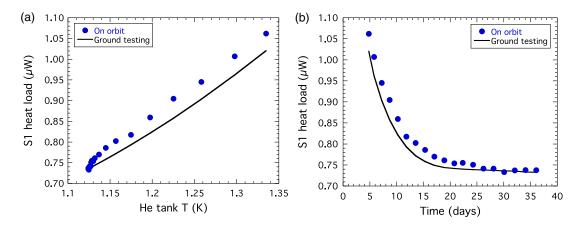
Fig. 7 Heat load on stage 1 for each ADR cycle on orbit as a function of (a) helium tank temperature and of (b) time on orbit. The solid lines indicate the expected heat loads at the indicated tank temperature or time based on ground testing.
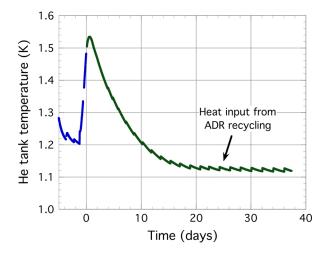
Fig. 8 Helium tank temperature from shortly before launch through to the end of operations on day 38. The increase leading up to launch was due to closure of the vent valve and periodically turning off the cryocoolers.

Fig. 9 Helium volume as determined from ADR recycles, compared with a direct measurement after the final top-off that was then integrated to reflect boiloff loss as the helium cooled. The solid line represents a loss rate of 0.024 L/day.

explanation fails on the grounds that the dewar main shell and internal shields all stabilized within a week of launch, at which time the heat load on stage 1 was still elevated. For microphonic heating due to vibration of the main shell (#3), the basis for concern is that the mechanical isolators supported the compressors off the main shell could have shifted during launch to create a mechanical short. In prior testing of the engineering model (EM) SXS instrument without the isolators, heating due to compressor vibration was strongly dependent on the degree of overlap between the exported vibration and resonant frequencies of the ADR and detector assembly. After launch, as the main shell and cryocooler radiators cooled, the vibration spectra of the cryocoolers could have changed and produced a time-variable microphonic effect. The main argument against this possibility is that the detectors exhibited none of the severe excess noise that was observed in EM instrument testing prior to installation of the isolators.

In summary, the source of the excess heating on stage 1 remains uncertain, and likely will remain so due to the limited on-orbit data available for assessing possible root causes.

3.4 Adiabatic Demagnetization Refrigerator Heat Rejection and Helium Tank Mass Gauging

As mentioned previously (Sec. 2.5), the heat output of the ADR was calibrated during ground testing by direct calorimetric measurements of the heat produced by each source within the ADR. The result was an ability to determine not only the total heat output to the liquid helium during a recycle but also the instantaneous rate. The latter can be reconstructed from control parameters included in telemetry from the control electronics, such as magnet charging voltages, heat switch getter temperatures (which dictate power dissipation and thermal conductances), and temperatures within the ADR that can be used to calculate heat flows. Thus, the heat flow model calculates heat flow based on the unique pattern of each recycle.

Since superfluid properties ensure that any heat input is distributed throughout the liquid and the liquid temperature remains uniform, an accurate model of the ADR's heat output combined with accurate measurements of liquid temperature (and its response to the heat input) can be used to determine
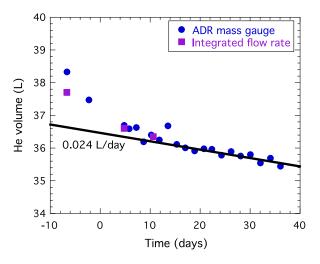
the amount of liquid present. Based on cross calibration of the ADR mass gauging technique with the standard method of using a known heater input for several fill levels, we estimate that the ADR technique has an accuracy of ∼0.2 L.

Figure 8 shows the helium tank temperature from 4 days before launch through the end of the mission. Periodic recycling of the ADR gives rise to the distinctive sawtooth pattern, with each recycle transferring about 11.7 J to the liquid. Averaging over the 48-h interval between recycles gives a time-average heat load to the liquid helium of 0.067 mW.

The mass gage analysis based on ADR cycles conducted during the 38 days of Hitomi's operating life is shown in Fig. 9. The mass values are shown compared with estimates of the liquid volume based on direct measurement using a superconducting level gage immediately after the prelaunch topoff, and integrating the boiloff losses during subsequent ground operations and mass loss inferred from cooling of the liquid on orbit.

The best fit to the liquid volume after steady-state temperature was reached, at about day 15, indicated a steady mass loss of 0.024 ± 0.0022 L/day. Under these conditions, which would have persisted as long as the cryocoolers remained operational, the liquid carried to orbit had an expected lifetime of 4.2 years.

4 Summary

The SXS instrument on the Hitomi x-ray observatory was launched cold, carrying ∼37 L of superfluid helium to orbit on February 17, 2016. On ascent, the valve that allows venting of the helium gas through the porous plug was opened.[16] During the first 2 days on orbit, the Stirling and Joule–Thomson cryocoolers were powered on, thus reducing heat loads on the liquid helium and accelerating its cooling to the point where ADR operations could begin.

On day 5, once the helium cooled below 1.4 K, the first ADR cycle was initiated by ground command. The first recycle took somewhat longer than usual—about 1 h—as both salt pills started warmer (1.4 K) than for subsequent recycles, requiring the rejection of more heat to reach the standard demagnetization point. Within a half hour of demagnetizing the two ADR stages to their operating temperatures of 0.5 K and 50 mK, the detectors were fully operational and recording x-ray events from

Table 2 Comparison of cryogen mode cooling requirements and performance of the three-stage SXS ADR during ground test and on-orbit operations.

		Performance	
	Requirement	Ground test	On orbit
Detector operating temperature (K)	0.05	0.05	0.05
Detector temperature stability (μK rms)	2.5	<0.5	2.0[a]
Detector housing temperature stability (mK)	1.0	<0.2	<0.2
Minimum observing efficiency	90%	>97%	>97%[a]
-Typical hold time (hours)	24	42	48
-Typical recycle time (hours)	1	0.75	0.75
Time-average heat load to the liquid helium (mW)	0.2	0.071	0.067

[a]Value excludes periods of time where the Hitomi orbit passed through the SAA.

external sources and an on-board Fe-55 calibration source. The detector resolution for all pixels was eventually verified to be the same as before launch, ~4.9 eV.[17–19]

Seventeen subsequent ADR recycles were commanded from the ground either as the ADR approached the end of its hold period, or earlier if needed for observatory commissioning activities. These activities included early observations of high-intensity celestial targets to verify proper detector operation before opening the dewar's gate valve to give the detector array an unobstructed view of the x-ray telescope. With the gate valve closed, the detector array could observe x-rays from the telescope only through a thin beryllium window that stops x-rays less than about 2 keV.

In all, 18 ADR cycles were conducted during the 38 days that the observatory was operational. Cooling of the helium to a final temperature of 1.125 K steadily increased the ADR's hold time to ~48 h. Recycling required ~45 min, yielding a duty cycle of 98.5%. When an equilibration time (~25 min) for the detectors to stabilize at 50 mK after a recycle is factored in, the SXS instrument achieved an observing efficiency of about 97%. However, a significant fraction of operational time at 50 mK was lost due to the effects of high-energy particles as the observatory passed through the SAA. During these passes, the temperature stability of the detector array could not be maintained at the required level of 2.5 μK rms.

In its totality, though, the SXS instrument was very successful in demonstrating both the detector technology and cryogenic cooling system needed to perform high-resolution imaging and spectroscopy of x-ray source. As a capsule summary, Table 2 compares the ADR's driving requirements in cryogen mode,

and the performance observed during both ground testing and on-orbit operations.

Unfortunately, on the 38th day of orbital operations, a series of attitude control issues resulted in the observatory entering into an uncontrolled spin, from which recovery was eventually judged impossible. Nevertheless, the last telemetry received shows Hitomi spinning with the solar arrays pointed away from the sun, but all systems within the SXS still operating normally.

References

1. K. Mitsuda et al., "The high-resolution x-ray microcalorimeter spectrometer system for the SXS on ASTRO-H," *Proc. SPIE* **7732**, 773211 (2010).
2. T. Takahashi et al., "The ASTRO-H mission," *Proc. SPIE* **7732**, 77320Z (2010).
3. K. Mitsuda et al., "The high-resolution x-ray microcalorimeter spectrometer, SXS, on Astro-H," *J. Low Temp. Phys.* **167**, 795–802 (2012).
4. Y. Soong et al., "ASTRO-H soft x-ray telescope (SXT)," *Proc. SPIE* **9144**, 914428 (2014).
5. R. Fujimoto et al., "Cooling system for the soft x-ray spectrometer (SXS) onboard ASTRO-H," *Proc. SPIE* **7732**, 77323H (2010).
6. S. Yoshida et al., "Flight model performance test results of a helium Dewar for the soft x-ray spectrometer onboard ASTRO-H," *Cryogenics* **74**, 10–16 (2016).
7. Y. Sato et al., "Development status of the mechanical cryocoolers for the soft x-ray spectrometer on board Astro-H," *Cryogenics* **64**, 182–188 (2014).
8. P. J. Shirron et al., "ADR design for the soft x-ray spectrometer instrument on the Astro-H mission," *Cryogenics* **50**, 494–499 (2010).
9. P. J. Shirron et al., "Design and predicted performance of the 3-stage ADR for the soft x-ray spectrometer instrument on Astro-H," *Cryogenics* **52**, 165–171 (2012).
10. P. J. Shirron et al., "Operating modes and cooling capabilities of the 3-stage ADR developed for the soft x-ray spectrometer instrument on Astro-H," *Cryogenics* **74**, 2–9 (2016).
11. G. A. Sneiderman et al., "Cryogen-free operation of the soft x-ray spectrometer instrument," *Proc. SPIE* **9905**, 99053N (2016).
12. M. Tsujimoto et al., "In-orbit operation of the ASTRO-H SXS," *Proc. SPIE* **9905**, 99050Y (2016).
13. Cernox (model CX-1030-CU) and germanium (model GR-200A-30) resistance thermometers are a product of LakeShore Cryotronics Inc., Westerville, Ohio.
14. P. J. Shirron, "Applications of the magnetocaloric effect in single-stage, multi-stage and continuous adiabatic demagnetization refrigerators," *Cryogenics* **62**, 130–139 (2014).
15. P. J. Shirron et al., "Thermodynamic performance of the 3-stage ADR for the Astro-H soft x-ray spectrometer instrument," *Cryogenics* **74**, 24–30 (2016).
16. Y. Ezoe et al., "Porous plug phase separator and superfluid film flow suppression system for the soft x-ray spectrometer onboard ASTRO-H," *Proc. SPIE* **9905**, 99053P (2016).
17. R. L. Kelley et al., "The ASTRO-H high-resolution soft x-ray spectrometer," *Proc. SPIE* **9905**, 99050V (2016).
18. F. S. Porter et al., "In-flight performance of the soft x-ray spectrometer detector system on ASTRO-H," *Proc. SPIE* **9905**, 99050W (2016).
19. C. A. Kilbourne et al., "The design, implementation, and performance of the ASTRO-H SXS calorimeter array and anti-coincidence detector," *Proc. SPIE* **9905**, 99053L (2016).

Biographies for the authors are not available.